

High-transparency clear window-based agrivoltaics

Mikhail Vasiliev^{1,*} , Victor Rosenberg¹, David Goodfield², Jamie Lyford¹, and Chengdao Li²

¹ ClearVue Technologies Ltd., Perth, Australia

² Environmental Technology Centre, School of Science, Technology, Engineering & Mathematics, Murdoch University, Perth, Australia

Received: 30 January 2023 / Accepted: 20 July 2023

Abstract. A number of modern glass and window products based on novel glazing designs, low-emissivity thin-film coatings, and proprietary fluorescent interlayer types have been developed recently. Advanced windows of today can control properties such as thermal emissivity, heat gain, colour, and transparency. In novel glass products, solar energy harvesting through PV integration is also featured, enabled by either patterned-semiconductor thin-film energy conversion surfaces, or by using luminescent concentrator-type approaches to achieve higher transparency. Typically, semitransparent and also highly-transparent PV windows are purpose-designed, for applications in construction industry and agrivoltaics (greenhousing), to include special types of luminescent materials, diffractive microstructures, and customized glazing systems and electric circuitry. Recently, significant progress has been demonstrated in building integrated high-transparency solar windows (featuring visible light transmission of up to 70%, with electric power output $P_{\max} \sim 30\text{--}33 \text{ W}_p/\text{m}^2$, e.g. ClearVue PV Solar Windows); these are expected to add momentum towards the development of smart cities and advanced agrivoltaics in greenhouse installations. At present (in 2023), these ClearVue window designs are the only type of visually-clear and deployment-ready construction materials capable of providing significant energy savings in buildings, simultaneously with a significant amount of renewable energy generation. The objective of this study is to place the recent industrialised development of ClearVue[®] PV window systems into a broader context of prior studies in the field of luminescent concentrators, as well as to provide some details on the measured performance characteristics of several ClearVue window design types deployed within the building envelope of a research greenhouse, and to elucidate the corresponding differences in their energy harvesting behaviour. An evaluation of the practical applications potential of these recently developed transparent agrivoltaic construction materials is provided, focussing on the measured renewable energy generation figures and the seasonal trends observed during a long-term study. This article reports on the measured performance characteristics of research greenhouse-based agrivoltaic installation constructed at Murdoch University (Perth, Australia) in early 2021. The solar greenhouse at Murdoch University has demonstrated great potential for commercial food production with significant energy savings due to on-site energy production from its building envelope.

Keywords: Window integrated PV / agrivoltaics / smart glazing / renewable energy

1 Introduction

At present, widespread energy innovations in terms of optimizing both the on-site distributed energy generation and the energy use intensity are urgently required in the built environment and in agricultural production facilities. This is due to the vast amounts of energy being consumed in buildings (more than 40% of the total nationwide energy consumption occurring in the US buildings sector already in 2018 [1]), and the necessity to de-carbonize the built

environments, preferably offsetting carbon emissions and materials-embedded carbon through the use of advanced materials capable of carbon offsetting in their installed “use phase”. New advanced construction materials combining the benefits of ongoing energy savings (e.g. in HVAC and also lighting) and on-site production of renewable energy using solar resources are urgently required. Ideally, these novel materials and products must be able to be integrated into the structure of either new or existing buildings, and be able to provide substantial energy benefits through occupying substantially large sun-exposed building envelope areas. Energy-generating energy-efficient solar façade materials can provide a substantial momentum for decarbonization of

*e-mail: mikhail@clearvuepv.com

the buildings sector, because of the much greater deployment-ready surface areas (typically by a factor of >10 , relatively to any conventional roof-mounted PV) which are available for solar-harvesting façade technologies. Effective, long-term decarbonisation of built environments is only possible if an optimized combination of all available solar generation technologies utilizing all possible building-envelope areas is deployed, providing near-net-zero operation capability while being integral to the building structure.

The development of high-transparency solar PV window products with climate-tailored thermal properties is expected to provide a useful pathway towards effective and widespread decarbonization in both the urban and agricultural (agrivoltaic) settings.

The building-integrated PV (BIPV) sector is growing fast, almost worldwide, deploying a broadening range of new technologies and products (detailed reviews are available, e.g. [2–9]), the majority of installed PV capacity growth still takes place in conventional installations (solar farms and rooftops). A new segment of PV industry enabling improved energy efficiency in agricultural production has recently emerged, known as agrivoltaics, where the optimised arrangements of partially-transparent PV and BIPV modules are required to balance the requirements of achieving energy savings simultaneously with maintaining crop growth productivity and land-use efficiency [10–12]. Efficient production of commercial crops in greenhouses requires maximum possible delivery of the photosynthetically active radiation (PAR, the wavelength range between 400–700 nm) to plant leaves, placing substantial constraints on the design of agrivoltaic installations, where the PV modules must be either highly-transparent, or occupy only a limited fraction of wall or roof areas. On the other hand, in commercial buildings, dependent on local climate, semitransparent BIPV window modules require multi-parameter optimisations, enabling the correct balance between the energy generation per unit area and energy savings. Therefore, engineering of the highly-customised and climate-dependent combinations of the thermal (insulation U-value), optical (visible transmittance and solar heat gain), and electric (W_p/m^2) properties are required to ensure wide acceptance of emergent BIPV technologies. Compared with conventional rooftop PV and most (even semitransparent) BIPV modules, where the semiconductor energy-converting components are typically only protected from the environment by ~ 3 mm thick coverglass, the window-integrated systems are expected to have longer useful lifetimes (of >30 years), due to the placement of semiconductor modules inside window compartments such as argon-filled spaces, and protected by thicker layers of glass from factors such as rapid temperature variations or strong UV exposure. At the same time, the relevant recycling procedures applicable to solar windows will be similar to these used with conventional PV and BIPV, since their main component materials (glass and semiconductors) are identical, or similar. A range of novel BIPV and high-transparency window-integrated PV (WIPV) products has been developed by ClearVue Technologies

(Perth, Australia) [4,13], already tested and proven to be suitable for deployment in both the construction sector and greenhouses.

ClearVue solar WIPV systems feature the following set of innovative features:

- Custom-designed energy-saving glazing systems utilizing special types of glass and low-emissivity coating(s) to provide substantial thermal energy savings in a range of deployment climates (adjustable SHGC, U-value, and visible light transmittance).
- Glazing-integrated luminescent solar concentrator (LSC) panel harvesting primarily the UV-blue and also the near-infrared solar radiation components while providing maximized visible light transparency and reducing the energy harvesting losses dependent on the incidence angles of solar radiation and weather conditions. LSC technologies have been reviewed in [14], and the details of their characteristic features, performance metrics, typical implementation designs, and recently-demonstrated benchmark results have been reported in [15–19], among multiple other literature sources dating back to the 1970 s.
- 3D-structured, custom-shaped, custom-interconnected energy harvesting PV surfaces placed around glazing perimeter regions [20], maximizing the visual transparency and further reducing the efficiency losses that would normally occur in conventional BIPV with increasing incidence angle of the incoming sunlight.
- Customized, installation-specific electrical interconnections circuitry involving combiner boxes and micro-inverters, enabling optimisation of the energy production from a large-scale building structure containing multiple solar windows.

Several recent showcase implementations of ClearVue high-transparency solar window technologies in built environments, including both the research-oriented and commercial agrivoltaic facilities are shown in Figure 1; some of the performance-related datasets obtained from these installations have been reported in [4,21,22].

The following sections of this article provide some background details on the development of clear energy-generating glazing technology, focussing on the recent results and energy harvesting-related measurement data obtained from Murdoch University agrivoltaic facility.

2 Background on the technology features and development of transparent window-integrated PV

In order to find innovative ways of designing semi-transparent solar windows of high power conversion efficiency (PCE) and improved PV Yield characteristics, not only novel functional materials but also modifications in the structure of PV-integrated glazing systems are required. Several novel and recently-developed approaches to the solar windows design utilising the latest results from the well-established field of luminescent



Fig. 1. High-transparency ClearVue solar windows deployed in commercial property-based and agricultural R&D and production facilities. Top: shopping centre atrium incorporating PV windows installed in 2019 in Perth, Australia; Middle: solar glazing-based greenhouse installation (2021) at Murdoch University (Perth, Australia); Bottom: wall of solar windows installed at a commercial greenhouse built in Sendai, Japan (image reproduced from Tomita Technologies website, 2022).

solar concentrators (LSC), in combination with recent developments in the materials science of thin films, luminescent materials, and photonics were reported in [17,18,21–27].

2.1 Principal characteristics and features of luminescent concentrator-type PV

The task of designing highly transparent LSC-type devices of relatively high PCE for BIPV and window applications involves considering fundamental trade-offs and theory limits described by Yang et al. [28]. It is possible to design LSC-type solar window systems featuring enhanced probability of the incident photons collection by the solar PV elements, simultaneously with enhanced quantum yield of PV conversion. LSC-type solar window designs typically rely on using custom-shaped, custom-connected PV energy conversion modules placed around the window perimeter and glass edge areas, with a fraction of the

sunlight incident onto clear glass area being redirected towards PV surfaces. This redirection of incident light can occur either through the internal light diffusion mechanisms (e.g., diffraction or scattering), or it can be engineered through luminescent downconversion (or even upconversion), where the majority of light rays re-emitted by the embedded luminescent particles at different wavelengths can be partially trapped within glass due to total internal reflection. Installing additional front-facing narrow PV modules near the system perimeter to face direct full-spectrum sunlight would effectively reduce the geometric gain factor, but meaningfully increases the overall light capture efficiency [21,22,29]. Utilising the luminescent downshifting (LDS) functionality by selecting the appropriate luminophore materials for use in transparent LSC can further increase the system PCE due to improving the spectral response matching between the solar cells and the wavelength-converted luminescent emissions [19,29–31]. In all solar window systems using PV modules installed under relatively thick layers of glass, whether facing the sunlight directly, or placed adjacent to glass edge surfaces at different location-specific angles to the incoming sunlight, there are significant efficiency losses observed due to the glass itself shading the solar cells, as well as due to the geometric design-related internal shading distributions existing invariably across parts of PV module areas. There is also a substantial angular sensitivity of the PV module's electric response to the intensity distribution of the incoming sunlight, especially when multiple (and relatively complex-structured) PV modules are electrically interconnected together to generate the combined solar window output. Regardless of the chosen interconnections circuitry details, different PV modules installed into a window (or even parts of the same multiply-connected PV subsystem at different sides of perimeter) can be mismatched electrically in either voltage or current, due to receiving non-identical light spectra or intensity distributions. These electric mismatches existing between parts of the combined PV module circuit of a solar window can strongly affect the shape of output $I-V$ curve characteristics, and can invoke the protective bypass diode circuits operation, ultimately limiting the module Fill Factor, and the window PCE. Therefore, considering all of the optical, materials-related, and electrical factors strongly affecting the system operation, a multidisciplinary design approach is needed to engineer practical LSC-type solar window devices capable of providing stable energy output and large energy yields in realistic deployment conditions.

It is important to note that the main performance characteristics of any LSC-type device are governed by equation (1), where G is geometric gain (the ratio between the light collecting front area of device to the area of near-edge, or edge-mounted cells), P is photon collection probability (the ratio of the number of photons escaping through glazing system edges to the number of photons incident onto front surface of concentrator). This quantity is often also called “optical efficiency”, however, some terminology-related disagreements still exist in the LSC-related body of literature, related to the definition of optical efficiency, with newer publications focussing on the external and internal photon collection efficiency. C_{opt} is optical power concentration factor; detailed definitions for

these parameters are available from [16,19].

$$C_{opt} = G * P. \quad (1)$$

In equation (1), the geometric gain is adjustable by the window system designer, and is largely governed by the window dimensions and the design of PV modules placed near window perimeter/edge areas to collect light. Typical values of G for $\sim 1\text{m}^2$ windows are between $\sim 5\text{--}10$, dependent on whether solar PV strips are also placed around backside perimeter near glass edges. The photon collection probability, on the other hand, is a function of core technology used within the LSC-type glazing system, especially the luminescent and/or scattering materials and components used, e.g. glass panes chemistry, heat-mirror-type optical coating(s), any diffractive elements, and the overall optical arrangement of these components. In most (or practically all) high-transparency large-area solar windows and LSC devices of different design types reported to date, the optical concentration factor C_{opt} quantifying the radiation flux density reaching the near-edge solar cells is less than unity (data tables containing relevant literature-reported figures of LSC performance parameters have been reported in e.g. [3,17]; the optical efficiencies demonstrated in most LSC devices to date were also modest (typically well below 10%, [19]). This is due to the fact that allowing a substantial fraction of total incoming visible-range sunlight energy through the window strongly reduces the energy available for the wavelength conversion and internal redirection. Luminescent materials can only convert a fraction of the available incident spectrum, with a finite quantum yield (QY); only quantum dot materials can currently compete with organic-dye pigments reaching $\text{QY} > (\sim 80\%)$; most of inorganic phosphor materials embedded into polymer matrices have QY limited to max. $\sim 40\%$, with very few of these featuring near-infrared excitation and/or emissions.

The refraction, multiple reflection, diffraction, and scattering-related light transport phenomena can also assist in improving the probability of photon collection by the energy-converting solar cell surfaces installed inside solar windows [24–26,32].

2.2 Recent development history of high-transparency WIPV

Large-area (200 mm × 200 mm, 500 mm × 500 mm, and larger) high-transparency solar windows employing glass-based glazing systems, customised low-emissivity coatings, and inorganic luminescent materials have been designed and demonstrated at Edith Cowan University (ECU, Perth, Australia) between 2012 and 2019. Oxide and sulphide-based rare-earth-doped phosphor particles excitable by the UV-blue and also the near-infrared solar radiation components, and featuring both the luminescent downshifting and upconversion-type emissions, were incorporated into epoxy-based lamination interlayers. Figure 2 provides an illustration of the lab testing methods used to optimize the luminophore compositions and concentrations in early (2012–2013) experiments with

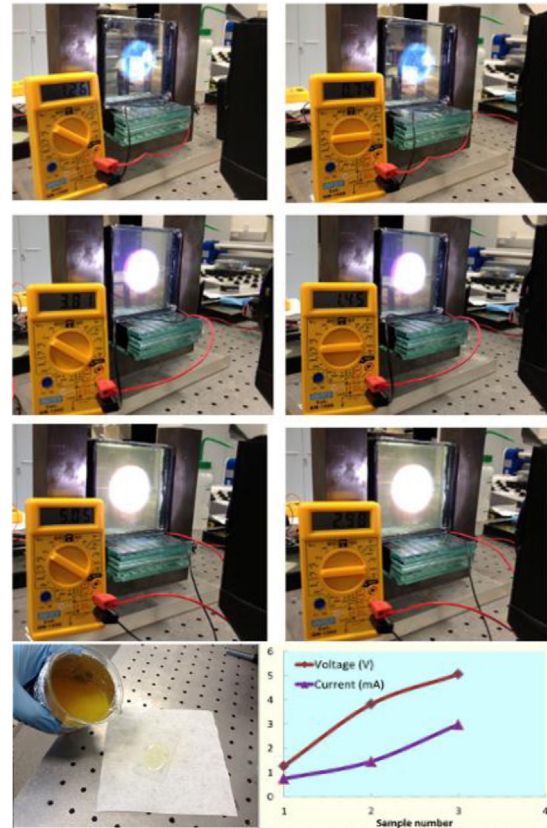


Fig. 2. Lab testing of 100 mm × 100 mm solar window prototypes (2012–2014) containing various interlayer compositions with different concentrations and chemistries of luminophore particles dispersed into UV-curable epoxy layers of $\sim 1\text{mm}$ thickness. The glass sample images are organized into three horizontal rows, each row containing the same solar window sample, but showing the measurements of either the open-circuit voltage (left), or the short-circuit current (right). Typical appearance of transparent fluorescent epoxy in its liquid state is also illustrated in the bottom row, together with the measurement results obtained from the three above-shown window samples irradiated by an identical solar simulator beam. Substantial variations in the measured electrical parameters correlated with the differences in the interlayer composition (more details available from Ref. [25]).

100 mm × 100 mm high-transparency glazing samples with four strip-shaped parallel-connected CuInSe_2 PV modules attached to glass edges. Measurement results (V_{oc} and I_{sc} measured with a collimated beam from a solar simulator incident normally onto glass surfaces) obtained from these (3 shown) different glass samples are also illustrated, together with a UV-curable epoxy sample, into which the luminophore particles were dispersed ultrasonically, prior to forming interlayers. The visual appearances of interlayers and glass also varied notably between the 3 samples shown, due to differing fluorescence intensities and light scattering strengths.

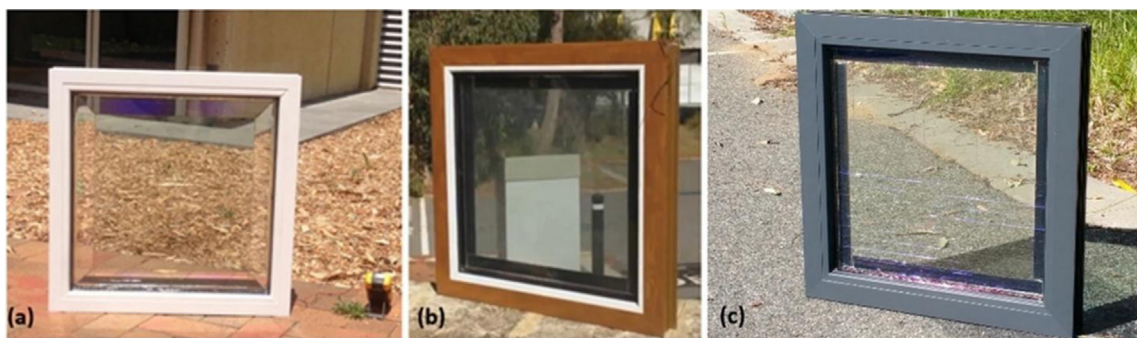


Fig. 3. R&D solar window prototypes (2014–2016) of various transparent solar glazing configurations of glass dimensions 500 mm × 500 mm. (a) Solar window with internal thin-film coated spectrally selective light deflectors using edge-attached PV modules only; (b, c) framed solar window prototypes using a combination of edge-attached and backside-perimeter PV modules, with an epoxy resin-based planar interlayer (b), or with added internally-structured transparent spectrally selective components (c). The images were reproduced from <https://www.nature.com/articles/srep31831>.

Significant differences in the electric output parameters were observed in experiments with a large number of 100 mm × 100 mm solar window samples, related to the differences in their interlayer compositions and structure (concentration-thickness products related to distributing different types and amounts of fluorescent particles in epoxy layers of varied thicknesses). These early experiments, which also included the PV characterization of differently constructed samples in natural outdoor sunlight, have enabled the simultaneous optimization of the electric output parameters and visual transparency levels in small-area solar window devices.

The early-development solar glazing samples packaged as framed installation-ready solar window prototypes dating back to 2014 are shown in [Figure 3](#).

The prototypes shown in [Figure 3](#) employed CIS (CuInSe₂) custom-shaped PV modules of nominal efficiency near 13%, and the PV strips were directly attached to glazing system edges and also (in some systems) were positioned around the backside glazing perimeter regions. The electric power outputs from smaller (200 mm × 200 mm) high-transparency low-haze samples using edge-attached 26 mm-wide PV strips reached up to ~0.7 W ($I_{sc} = 72$ mA, $V_{oc} = 16.8$ V, $FF = 0.57$, measured at peak orientation in outdoor sunlight). In 500 mm × 500 mm internally-structured window samples similar to [Figure 3a](#), the electric outputs reached about 3W; windows of same dimensions featuring backside-perimeter CIS PV demonstrated electric outputs of over 5W in natural sunlight conditions, dependent on the internal glazing structure design. The performance characteristics of first factory-made ClearVue solar window designs also featuring CIS PV back in 2016–2017 in outdoor test installations have been reported in [\[21\]](#).

The luminescent material selection criteria, some types of functional material compositions potentially suitable for enabling improved energy harvesting performance in windows, sample measured spectra of luminophores featuring giant Stokes shift, and visual examples of transparent luminescent concentrator prototypes employing inorganic phosphor particles dispersed inside glass lamination interlayers are shown in [Figure 4](#).

Work is ongoing at multiple research groups worldwide on the design of LSC using giant Stokes shift inorganic phosphors capable of avoiding the well-known reabsorption problem, which is another limiting factor in large-area LSC design. Another factor of special relevance to the industrial production of solar windows is the necessity to develop suitable and reliable technologies for the incorporation of inorganic phosphors (or semiconductor nanocrystals) into the glass-based industry-standard window designs, without causing strong haze, colouration, and preferably avoiding the use of polymer slabs and any organics-based media not proven to provide decades-long lifetimes of solar exposure.

To the best of our knowledge, no other research group have so far demonstrated the industrialised development of high-power (tens of W/m²), clear, and size-scalable solar windows and published (e.g. Ref. [\[13\]](#)) flash-lamp PV I – V curve testing results for large-area (>1 m²) high-transparency glass-based clear and building standards-compliant solar windows (e.g. certified by IEC, UL, CE). In particular, the measured performance data for product-level windows demonstrating Ampere-scale currents at the maximum-power point, with large corresponding system voltages (V_{MPP} near ~50 V) and transparency levels exceeding 50% have not been so far published by any competitors. Our most recent development results in large-area (1.91 m × 0.95 m) solar windows (exported to Japan and installed at a commercial greenhouse in Sendai, built by Tomita Technologies demonstrated electric power outputs (measured at STC) of up to 50.5 W_p (27.83 W_p/m²), proving both the scalability of technology and product development progress. Compared with the commercially available Clearvue solar windows of size 1.2 m × 1.2 m made 1–2 years ago, the current (2021–2022) window models of the dimensions 1.1 m × 1.2 m have shown the I_{sc} improvements of up to 16.7% (~880–980 mA vs ~800–840 mA previously, at the same V_{oc} and FF), as recently measured at standard test conditions and also in field testing experiments. Clearvue windows generate their maximum power output at the optimised incidence-angle conditions, with the best incidence geometry being different from normal incidence. The latter feature

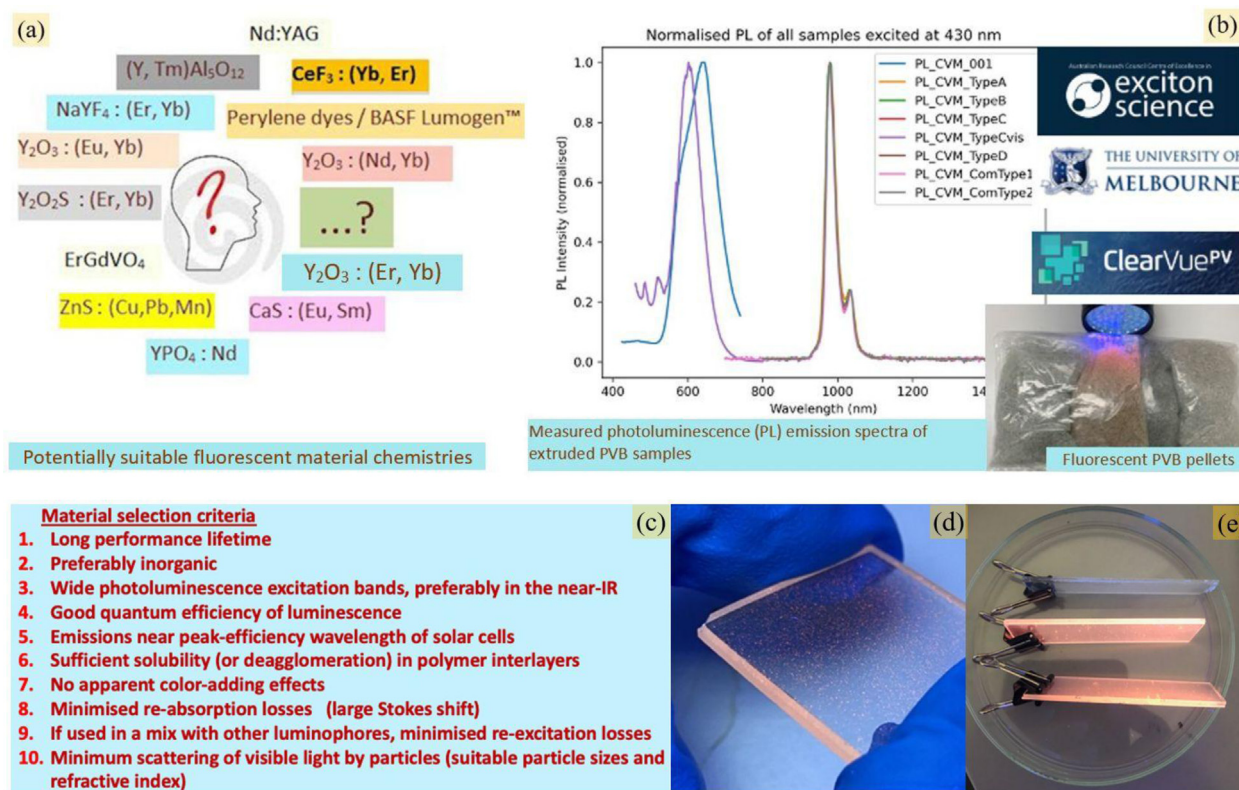


Fig. 4. Materials-related aspects of high-transparency solar window design. (a) Example types of inorganic luminophore chemistries potentially suitable for developing solar window devices; (b) photoluminescent emissions spectra of different functional materials embedded into extruded polyvinylbutyral (PVB) sheets measured by our cooperation partners at the University of Melbourne; (c) luminescent material selection criteria applicable to the design of luminescent solar concentrators; (d) high-transparency laminated glass samples linked by prototype fluorescent PVB interlayers demonstrating the visible component of fluorescent emissions concentrated at glass edge; (e) glass concentrator samples laminated using fluorescent PVB, shown under UV irradiation and also in comparison with a glass sample laminated using conventional PVB.

(not reported in any conventional PV modules) makes Clearvue solar windows particularly attractive for BIPV applications on vertical façade and wall areas. Current generations of ClearVue solar window designs rely on using custom-assembled, custom-interconnected mono-Si solar cell modules. Figure 5 shows the $I-V$ curve and power-voltage curve measurement results obtained from $1.1\text{ m} \times 1.2\text{ m}$ ClearVue solar windows of single-interlayer low-haze design type corresponding to the windows installed in Grow-Room #4 at Murdoch University Greenhouse.

Optimisation of solar window performance in terms of ensuring high transparency, largely colour-free and haze-free appearance, while maximising the electric output per unit module area is an active area of multidisciplinary research. Key new advances in this area are expected to result from the ongoing optimisations of inorganic luminescent material compositions and concentration-thickness products, glazing system structure and its components, and the improvements of customised PV modules and associated electrical circuitry details.

3 High-transparency window-integrated agrivoltaic installation at Murdoch University, Western Australia

A recent (2021) installation example of Clearvue solar windows is Murdoch University Solar Greenhouse (Fig. 6), in which 3 out of 4 grow-rooms ($\sim 50\text{ m}^2$ floor area each) were built using solar windows on the north wall, on the 20-degree tilted north-facing roof, and also on the west-facing wall. The greenhouse is located in Perth metropolitan area, at a southern latitude of $32^\circ 04'24''$. 153 solar windows in total represented an installed capacity of near 6.1 kW_p , which has led to strongly offsetting the running costs of greenhouse during 2021 in terms of HVAC system operation. Measurement data obtained from this greenhouse provided multiple insights into the potential benefits of using Clearvue solar windows in controlled-environment crops production, as well as the energy generation performance trends of different solar window design variations.

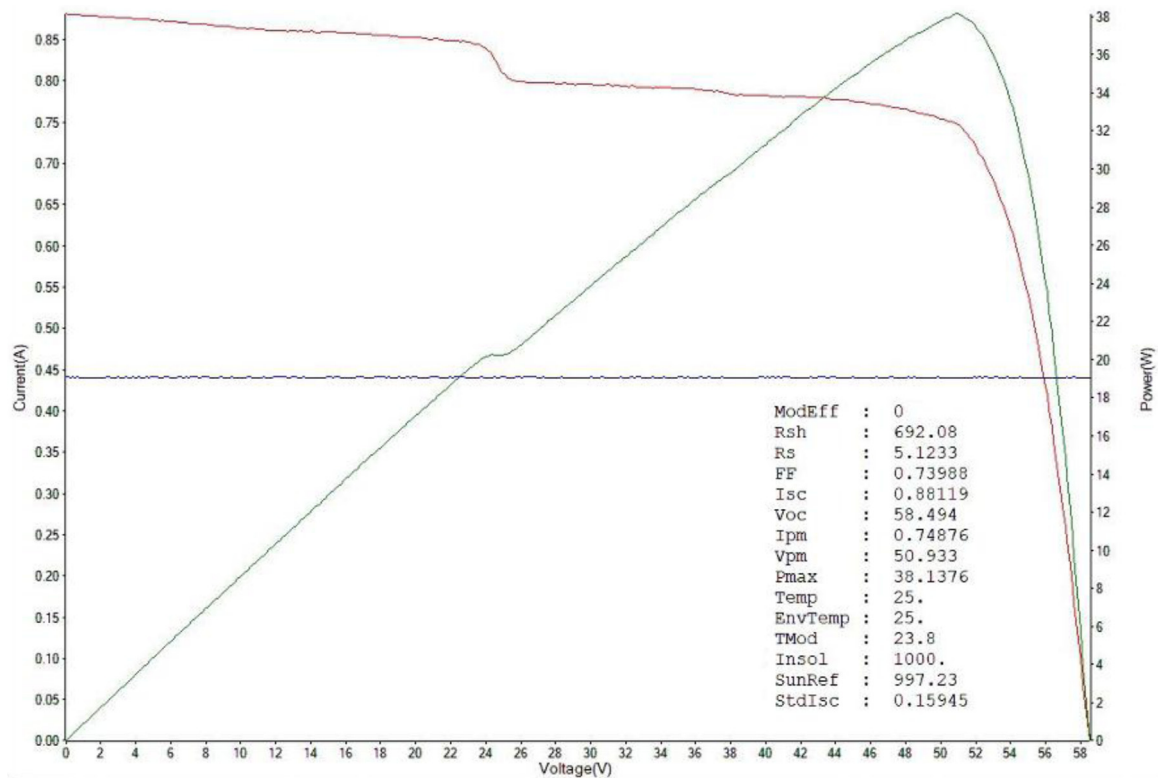


Fig. 5. Flashlamp standardised PV I – V curve measurement results obtained from $1.1\text{m} \times 1.2\text{m}$ ClearVue solar windows of single-interlayer low-haze design type corresponding to the windows installed in Murdoch University Greenhouse Grow-Room #4. The I – V curve (red trace), the power–voltage curve (green trace) and the measured PV performance dataset obtained from these windows demonstrated approx. $29\text{ W}_p/\text{m}^2$ rating at the standard test conditions at normal incidence. Blue line is a measurement system display artefact (and is redundant).

3.1 Greenhouse design features and measured performance characteristics

The greenhouse was designed to enable performance comparisons between four different grow-rooms, in terms of the energy consumption, energy production, microclimate stability, and crop growth productivity. Grow room #1 was glazed with standard low-iron ultraclear glass (2.4 mm-thick panes laminated using standard 0.76 mm PVB interlayer). Grow rooms 2, 3, and 4 were glazed with Clearvue solar windows, which featured identical triple-glazed window designs, but the 3 window types had slight differences in the PVB interlayer compositions and sequences used within their middle panes (made of three 4 mm-thick low-iron glass plates linked by two interlayers). Figure 6 shows the greenhouse design sketch and some climate control-related data collected prior to, and after the commissioning of automatic internet-of-things enabled climate control system.

The microclimate in each grow-room was finely controlled using a custom-designed HVAC system, keeping the temperature setpoints within $\pm 2^\circ\text{C}$ to optimise the plant growth. Even with this fine control of microclimate applied continually over the seasons, the PV installation has offset approximately $\sim 40\%$ of the total energy costs in Clearvue grow-rooms. Immediately following the greenhouse construction and fit-out, and prior to installing the

control algorithms running the HVAC systems, a thermal insulation performance comparison test was made, by way of recording the mean air temperatures in each room and its daily variations (Fig. 6d). The results showed that Clearvue-glazed grow-rooms remained several degrees warmer during the night, compared to the control room #1 glazed with plain glass; and during the daytime the air temperature rose at a much slower rate in all solar grow-rooms, due to the differences in the solar heat gain and thermal insulation U -values. The grow-rooms 1 and 4 initially had additional sunlight and thermal exposure aspects on the east and west walls of greenhouse, compared to the internal rooms 2 and 3; these exposure differences were minimised prior to running the characterisation and plant-growth experiments by installing thick Styrofoam screens on the inside of the eastern and western glass walls. The photovoltaic performance of the 21 solar windows installed onto west-facing wall of greenhouse was monitored separately and was not a part of the present study.

The PV installation contained 13 Enphase IQ7+ microinverters, each of which was connected to a parallel bundle of 12 windows (except one was connected to 9 windows); the system has been configured for exporting energy to the grid, with the measured self-consumed energy fraction typically being near 70%. The amounts of solar energy harvested by the solar windows installation at Murdoch University Solar Greenhouse (Building 899) were



Fig. 6. Greenhouse installation details and room temperature-related data. (a) Solar greenhouse at Murdoch University with grow-room boundaries marked. Room 1 is glazed conventionally using single-pane 8mm thick laminated glass; rooms 2–4 are glazed with Clearvue solar windows of 3 slightly different design types. The direction towards geographic North is shown with arrow, coincident with the direction of normal to the plane of front wall; (b) internal view from grow-room #4; (c) mean (volume-averaged) room air temperature datalogs recorded on June 14th and 15th, 2021 with HVAC control system running; (d) mean (volume-averaged) room air temperature datalogs recorded in April 2021, without HVAC control system running.

data-logged continuously, enabled by Enphase Enlighten online data interface processing the data from each of the 13 Enphase microinverters connected to parallel-bundled solar window arrays. Continuous observations of the logged power and energy data were made throughout 2021–2022, and the observed energy generation trends were also analysed in comparison with a reference conventional (roof-based, optimally tilted) 6.6 kW_p rooftop PV installation located in Perth metropolitan area. This reference roof-top PV installation is facing the north-western direction and is tilted at 22.5° to the horizontal plane. These orientation and tilt angles are the parameters required for achieving the optimised year-round PV energy production in Perth, considering the local latitude and the applicable local industry-standard roof pitch angles.

Figure 7 shows the comparative energy generation trends observed during autumn and winter seasons of 2021. A long-term daily energy generation datalog recorded from an array of 12 windows mounted on the roof of grow-room #3 is also shown, revealing the absence of any significant performance degradation and a relative stability of daily energy outputs throughout seasons.

It can be noted from the data of Figure 7b presenting the long-term performance of a roof-mounted 12-window array, that throughout all seasons, the minimum rainy-day daily energy outputs were typically not below ~30% of a peak-day production for each corresponding week of year. Compared with the summer-time daily energy production data also available from the same reference rooftop PV system, the seasonal variations in the daily energy outputs were smaller

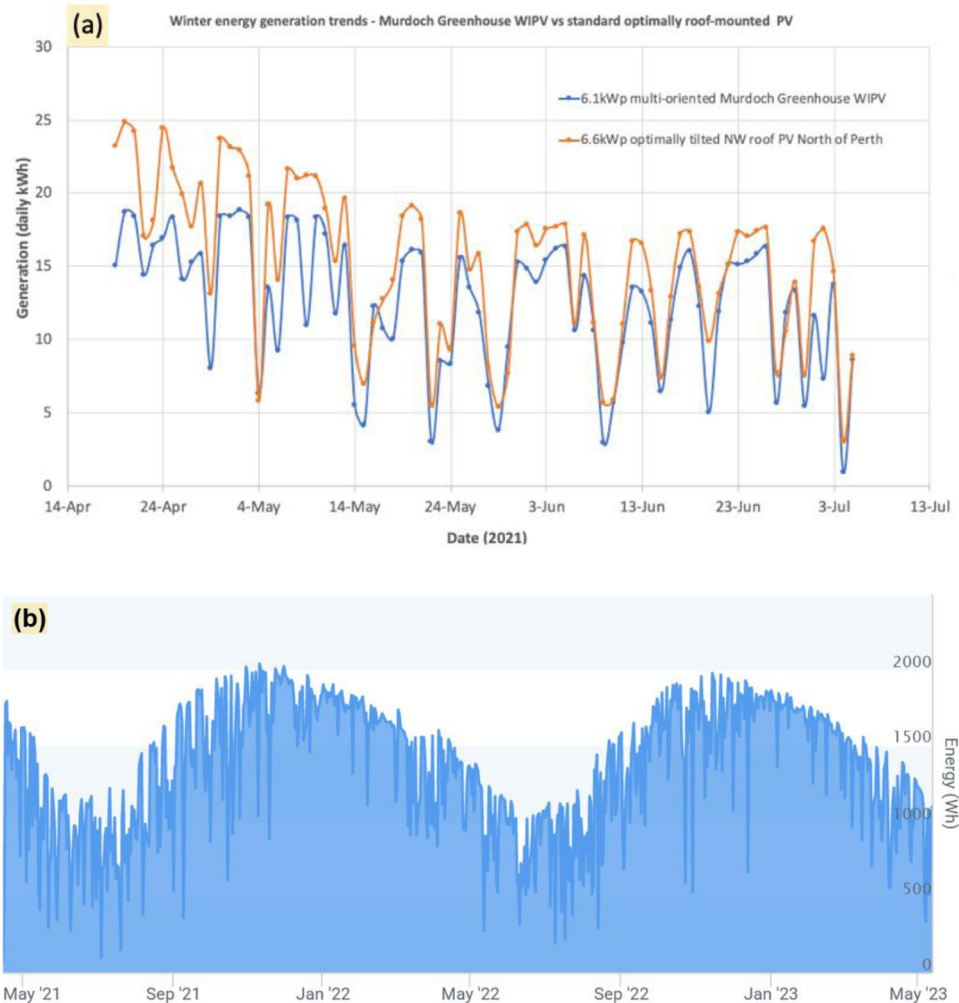


Fig. 7. (a) Solar PV energy generation trends measured during winter of 2021. Murdoch University Solar Greenhouse installation performance shown in comparison with an optimally-tilted, conventional rooftop PV installation in Perth. Data sources: Enphase Enlighten data (greenhouse), and Fronius Solar.Web app (home PV system owned by Dr M. Vasiliev); (b) long-term daily energy generation dataset recorded from an array of 12 windows mounted on the roof of grow-room #3.

on greenhouse roof. On sunny days, the greenhouse roof (Array G, roof of room #3) production from solar windows varied from approximately ~ 1.1 kWh/day in winter, to ~ 2 kWh/day in summer. The season-dependent daily energy production variations of the reference 6.6 kW_p conventional monocrystalline silicon-based rooftop PV system were larger, from approximately ~ 17 kWh/day on peak days in winter, to ~ 40 kWh/day on peak days in summer.

The energy harvesting performance of various types of solar PV installations in the “real-world” operating conditions (as opposed to the standard laboratory flash-test testing conditions (STC)) remains an area of active research [33,34]. Each PV system responds to its own uniquely local operating environment and its limitations, especially the external shading conditions, and the local climate type and its variations. It is well known that in the case of BIPV, where the installations often invariably involve multiple and non-optimum tilt angles (e.g. vertical walls) and azimuth orientations, significant (and season-dependent) discrepancies may be expected between the

modeled energy outputs and actual measured system performance.

Our main findings over the autumn-winter of 2021 were that Murdoch University Solar Greenhouse performed as expected, despite having a large area of vertically oriented windows (e.g. at North and West Walls), and on some rainier days even outperformed a standard 6.6 kW_p PV panels installation on an optimally tilted roof area (considering the installed PV capacity difference; data shown in Fig. 7). Both the North and West wall areas performed as expected (or better, particularly on some wall areas in the summer months of 2021-2022), considering the non-optimum orientation/tilt angles, as well as the weather conditions during the winter of 2021. The energy amounts harvested daily approached ~ 19 kWh/day. Some energy harvesting limitations were also observed, arising due to the maximum AC power output limitations of microinverters used, and affecting primarily the roof-mounted arrays on summer days. The data of Figure 7 confirms that Clearvue solar windows are particularly

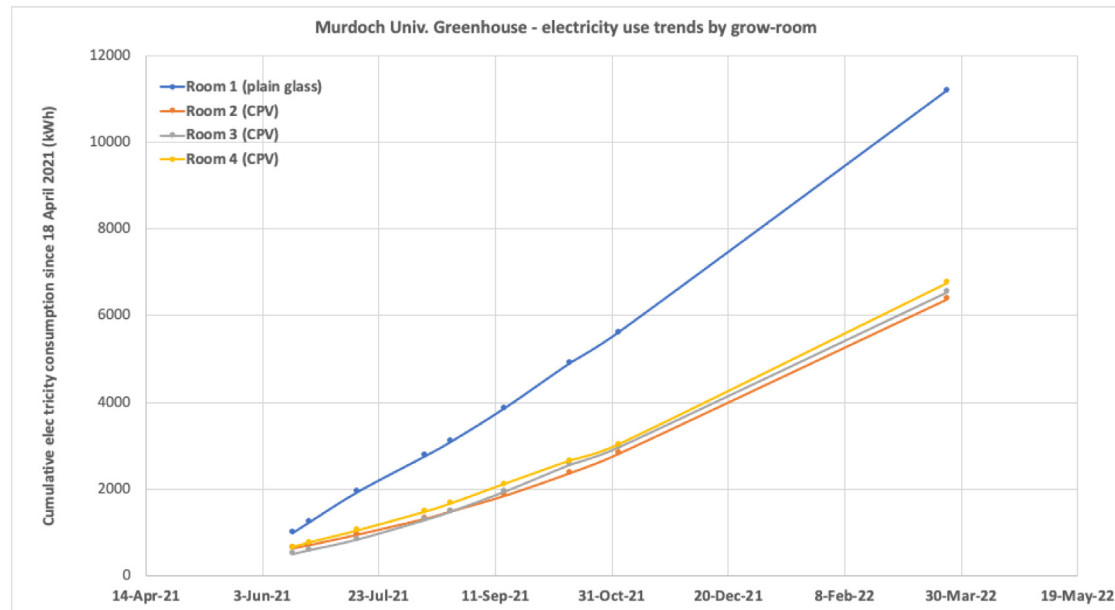


Fig. 8. Electric energy consumption trends in Murdoch University Solar Greenhouse grow-rooms observed during 2021–2022.

suitable for efficient solar energy harvesting in adverse environmental conditions (e.g. during rainy winter days), even when installed at a range of different azimuth and tilt angles. This finding was expected, due to the window design features providing the capability of capturing the incoming sunlight energy from a wide range of incidence angles.

Significant energy savings were demonstrated in greenhouse grow-rooms fitted with Clearvue solar windows, which demonstrated approximately 40% of total (season-averaged) energy self-sufficiency, due to the renewable energy generated. Figure 8 shows the measured electric energy consumption trends in all 4 grow-rooms, on a time scale of almost 1 year. Further optimisations to be applied to the internet-of-things (IoT) based HVAC control algorithms, involving more efficient air cooling applied through high-pressure evaporation of water mist, are expected to further improve the energy self-sufficiency, reducing the running time of high-power reverse-cycle air conditioners.

As was expected, conventionally glazed Room1 used electricity at a significantly higher rate, compared to solar grow-rooms, due to its significantly larger (by almost 30%) solar heat gain coefficient. Marginal (few %) energy use differences were noted between grow-rooms fitted with solar windows, possibly also correlated with their (slight) solar heat gain differences. The 3-monthly averaged energy self-sufficiency level (for all 3 CPV rooms) was equal to: PV generation total/total energy used = 1165 kWh/3082.42 kWh = 37.8% – averaged between 16 April to 21 July 2021, with the record rainy June and July months in 2021. On the other hand, during the same 3-month period, the ratio of total energy generated in Rooms 2, 3, and 4 to the metered grid-imported energy was as high as 49.7%. The costs of importing from grid (only ~ 2.3 MWh in 3 months' time)

were ~\$AUD 300/month, using off-peak Perth tariff of \$0.3896/kWh) indicate small running costs, compared to e.g. the expected running costs of energy in other R&D greenhouses at Murdoch Campus.

Figure 9 shows the remarkable stability of the monthly energy output from a 12-window array mounted vertically on the north-facing wall of greenhouse (Array F, with 7 windows on wall of room #3 and 5 windows on wall of room #4).

Despite significant Sun altitude angle variations occurring throughout seasons, no reductions in monthly energy output were recorded during the summer months; whereas a conventional PV panel-based vertical wall-mounted installation would be expected to reduce the energy production noticeably during summer, due to geometric factors. Figure 10 shows the results of the summer-time PV Yield comparison made with a conventional PV (or BIPV) system installation of identical installed capacity placed onto a north-facing vertical wall in Perth. The energy production data for December 2021 from Enphase Envoy interface showed a 53.4% energy production increase, compared to that expected from a conventional PV installation of same capacity.

Similar PV Yield comparison results for the wall-based windows were also observed in other months (e.g. November 2021 and January 2022, and also December 2022, when the weather was at its most stable for Perth). The PV Yields exceeding these available from conventional BIPV systems were expected, due to the design of Clearvue windows featuring the reduced angle-of-incidence sensitivity of electric power output, simultaneously with peak-output window orientation being slightly away (by 15–20°) from normal incidence. This makes these solar windows attractive for the (intrinsically multi-oriented) BIPV installations.

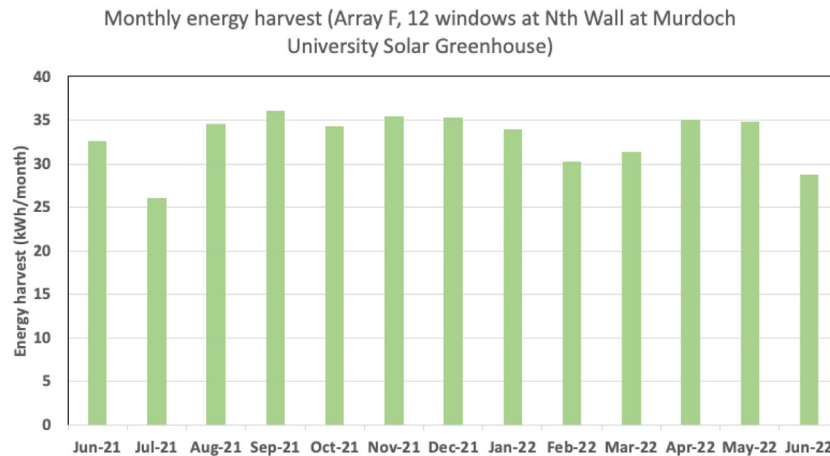


Fig. 9. Monthly energy production by a 12-window array mounted vertically on the north-facing wall of greenhouse.

3.2 Energy harvesting performance differences measured in PV windows of different interlayer design types

The designs of solar windows installed in 3 Clearvue grow-rooms slightly differed in terms of the number of luminescent material-doped polyvinylbutyral (PVB) lamination interlayers used and the concentrations of these materials distributed inside the polymer interlayers. Two differently-doped PVB designs were used, namely (1) “PVB-1” of lower doping concentration for higher-clarity windows, and (2) “PVB-2” of slightly higher luminescent particle concentration. No substantial haze-related visual clarity or appearance differences were noted between windows of different design modification. This was due to the rather modest concentrations of functional materials incorporated into both types of 0.76 mm thick PVB, being below ~ 0.1 wt.%. The following interlayer design differences related to the glazing design differences between grow-rooms 2, 3, and 4:

- Room 2 windows used two slightly higher-haze, but identical interlayers (“PVB-2” + “PVB-2”).
- Room 3 windows used two differently-doped interlayers (“PVB-2” + “PVB-1”).
- Room 4 windows used a single fluorescent interlayer (high-clarity “PVB-1”), with the other interlayer being “Ordinary PVB”.

Two PVB interlayers were needed to laminate the inner pane (integrated LSC-type panel) of each triple-glazed window system; each inner pane was itself composed of three 4 mm-thick low-iron glass plates. During the initial (pre-installation) field testing of all windows conducted at Murdoch Campus in February 2021 in outdoor natural-sunlight conditions, some performance differences between different window design types were noted, even though testing at standard test conditions (STC) could not be then performed, and the factory flash-lamp STC tests revealed only marginal (few %) peak power-output differences when measured at normal incidence angle. When measured at the optimised (by way of measuring the short-circuit current I_{sc}) angles of incidence, and at peak outdoor

sunlight irradiation, the windows (expectedly) showed the same open-circuit voltages near 61 V, however, the measured I_{sc} values differed systematically from ~ 840 – 860 mA in windows of Room 4, up to ~ 950 – 980 mA in windows designed for installation in Rooms 2 and 3. Therefore, the solar energy harvesting performance was expected to also differ by up to $\sim 10\%$ between the extremely-low-haze Room 4 and other Clearvue rooms.

The Enphase Enlighten online data interface allowed to map the PV energy production of all individual PV arrays (bundles of parallel-connected solar windows distributed over the greenhouse building envelope). Thus, the total energy production at different sections of greenhouse could be monitored online. Due to the electrical system design-related and geometric constraints of this agrivoltaic installation, it was not possible to install all separate 12-window PV arrays mounted on identically-oriented surfaces and using identical window design types. Instead, we ensured (to the extent possible, since some windows also required replacement during the construction process) that windows installed in each grow-room featured the same glazing design variation. However, most 12-window arrays featured a combination of wall- and roof-mounted windows, often extending over 2 different rooms per array. The power generation on roof areas would have been more strongly affected by factors such as weather-induced soiling and (during warmer seasons) the microinverters AC output limits, compared to the wall-mounted windows. Figure 10 shows the electric design schematic of the distribution of different north-facing PV arrays placed over the window and roof areas in all 3 solar grow-rooms, with roof and wall areas shown in separate diagrams. Array B had 3 windows placed onto north wall and another 9 on the west wall; Array A (not shown) was also placed on west wall. The web interface allowed energy production and power generation data collection summarised over user-defined time-frames.

The vertical wall areas are better representative of BIPV-deployed system energy yield performance, due to the expected reductions in energy amounts harvested, compared to roof areas, and also due to relatively smaller area contamination induced by weather. The wall-mounted PV windows were also expected to be less affected by the

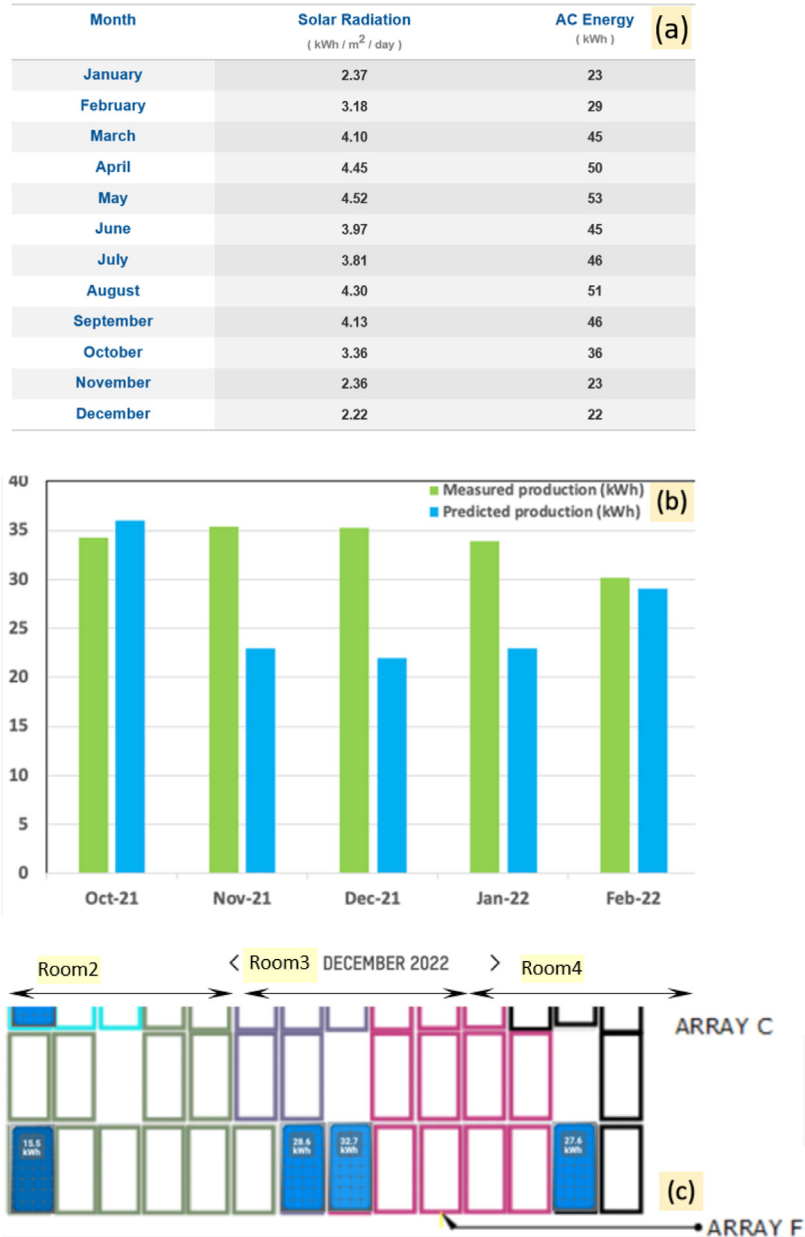


Fig. 10. Measured monthly energy production of a 12-window bundle (Array F, producing 35.3 kWh in December 2021) mounted on a north-facing vertical wall of Murdoch Greenhouse versus the predicted monthly energy output (23 kWh) of a conventional PV or BIPV installation of identical installed capacity ($0.4752W_p$) also mounted in the same geometric orientation, in Perth climate. (a) Monthly AC energy production data predicted by NREL’s PVWatts calculator, using installed generation capacity identical to that of Array F; (b) measured monthly energy harvest (Array F, during summer of 2021–2022) versus the predicted amounts; (c) monthly energy output of the same Array F recorded during December of 2022 (among other north-facing wall-mounted window arrays, last 3 windows from Room 4 not shown); the dataset is reproduced directly from the graphical output of Enphase online interface, confirming that the same energy output trend was maintained by Array F during late 2022, compared with the data from parts (a) and (b).

temperature-induced efficiency variations, due to their placement closer to ground level (in contact with cooler layers of greenhouse air), and receiving less direct incoming solar radiation flux per unit area. Long-term north-facing wall windows performance averages were observed between the different rooms of greenhouse between 16 April 2021 and 21 October 2022 (cumulative energy production data for this period are shown in Fig. 11).

Array *J* windows data were representative (11/12 windows) of Room2 (*N*th Wall) energy harvesting performance during the long-term observation period (18 months), amounting to 41.83 kWh/window.

Array *F* (split between Rooms 3 and 4 on the north wall, with 7 windows being of Room3 glazing design, and Array C (split between the *N*th Wall and roof of Room4) provide the reliable estimate for the long-term comparative data

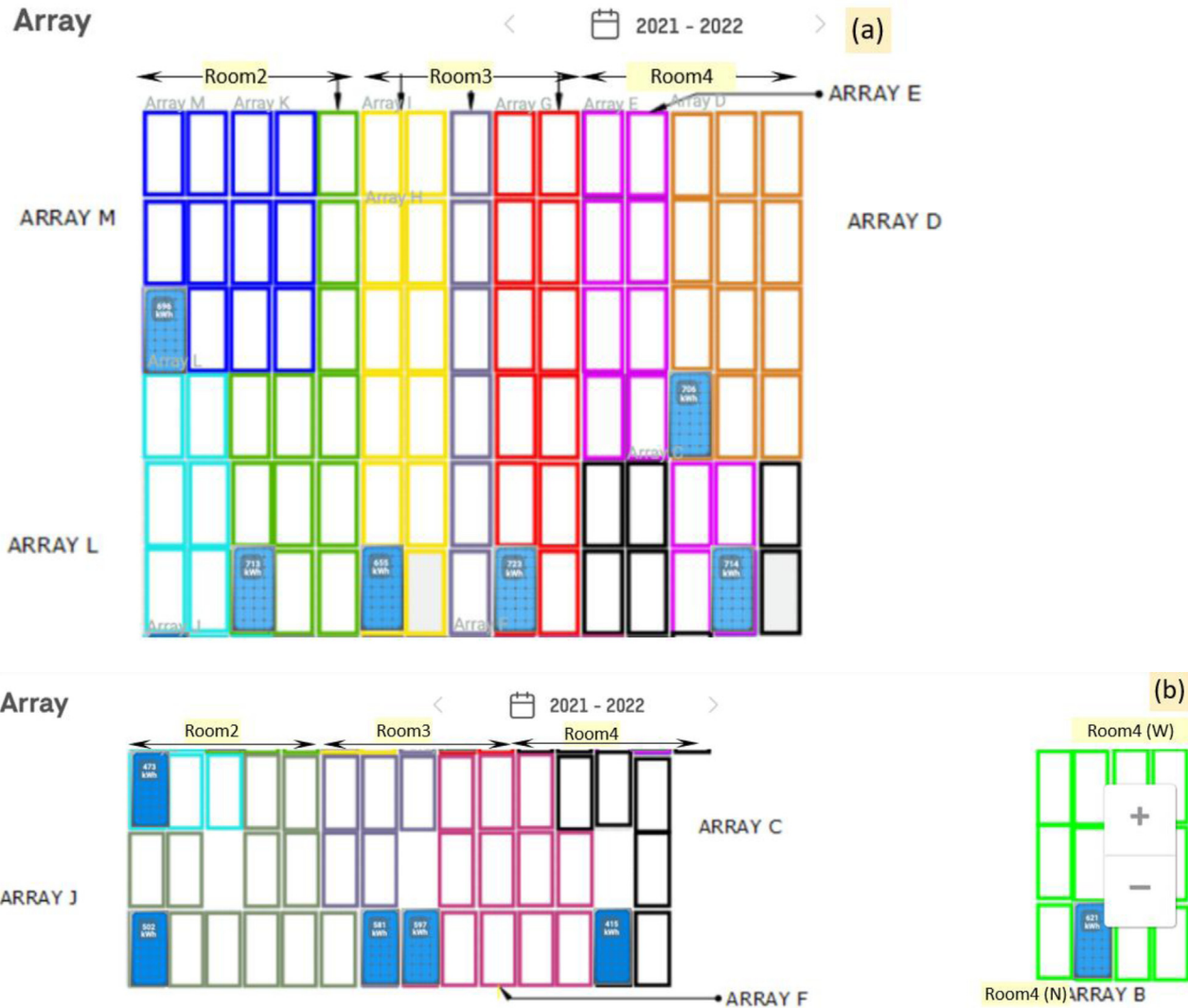


Fig. 11. Roof-mounted arrays (a) and *N*th Wall arrays (b) long-term energy generation data. (Note that the north-facing Array C long-term production figure was actually 621 kWh, erroneously swapped in the installer’s array diagram with Array B production data (415 kWh)). Each of the grow-rooms (2, 3, and 4) had 5 vertical columns of solar windows installed across the north-facing wall and roof areas; the wall height was 3 rows of windows. A conventional louvre-type window was placed in the middle of solar-window wall in each room, shown as clear space in diagram. 12-window Array A from the west-facing wall is not shown.

trends for different window design types. Given that the long-term average rooftop generation per window on roof of Room4 was 59.167 kWh/window (data from roof-based Arrays D and E), the total contribution of 6 wall-mounted windows of Array C (Room 4) can be derived to be $(621 - 6 \times 59.167) \text{ kWh} = 265.99 \text{ kWh}$, or 44.33 kWh/window.

The 12 windows of Array J (Room 2) generated only ~41.83 kWh/window (~5.6% less than wall windows of Room 4), however, there were vehicles occasionally parked (during peak insolation hours) outside and near the wall of Rooms 1 and 2; strong external shading effects could have been expected, possibly affecting the generation data of Room2 northern wall.

The 12 windows of Array F (mainly belonging to Room3 glazing design type, with some (max. 2) windows on the Room 4 part of Array J also being replaced during construction with

the windows of Room3 interlayer design type) generated 49.75 kWh/window during the observation period. These data suggest the minimum long-term energy-harvesting out-performance of Room3 Nth-wall windows, compared with Room4, to be ~12%. This figure also correlates well with the original field performance evaluation tests performed in February 2021, prior to the installation of solar windows into greenhouse structure. Array F windows have also consistently demonstrated significant PV Yield performance differences during warmer months (compared with the predicted energy yields calculated using a conventional-PV-based model, based on installed capacity, physical orientation, and local climate). Array J windows performed substantially weaker than Array F during summer months, but also performed similarly to Array F during winters; the exact reason for these

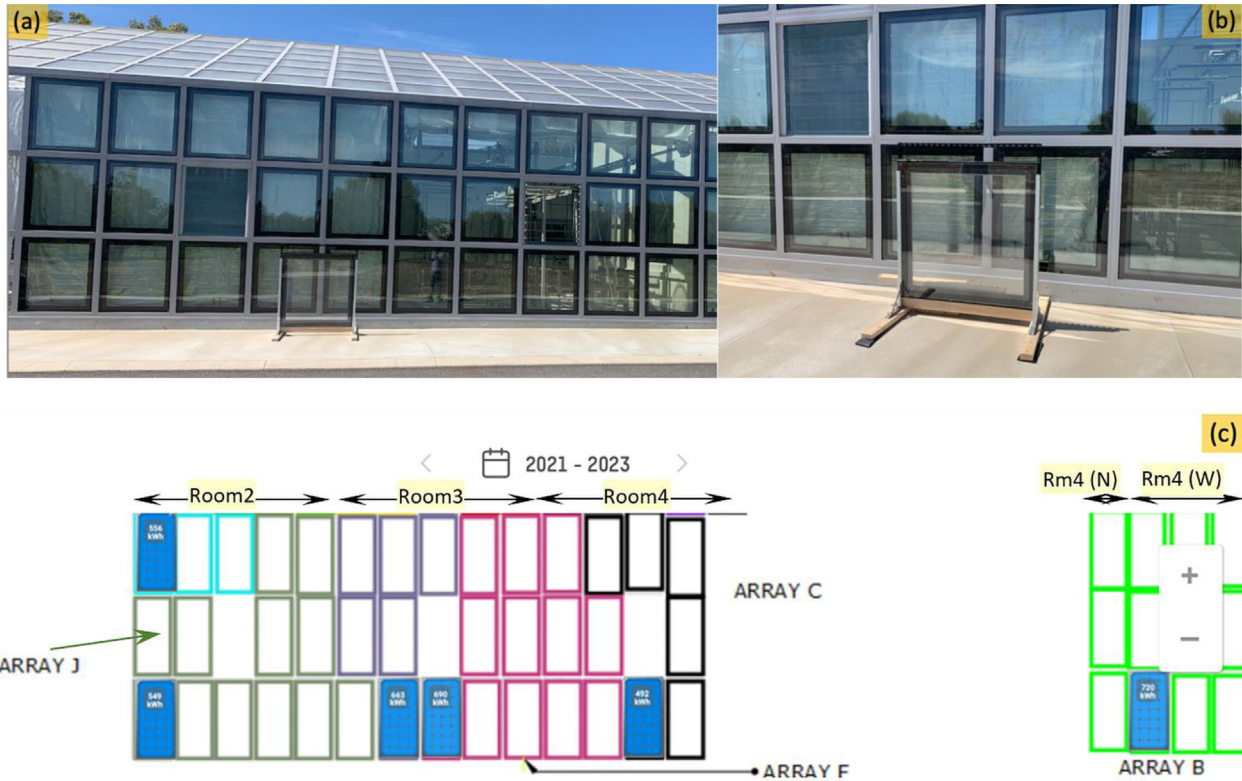


Fig. 12. (a, b) Energy harvesting testing arrangement enabling daily comparisons of energy produced by the test window and wall-mounted solar windows of other design types. The Test Window was connected to Victron 75/10 charging regulator using a 12 V battery in bulk charging mode as energy sink. (c) Wall-based PV arrays closest to the test window (12-window arrays J and F, and 6 of the wall-mounted Array C windows out of total 12). Empty white rectangles on diagram indicate non-solar windows used for room ventilation. The lifetime array generation data are shown for the period between 15 April 2021 and 18 January 2023; 720 kWh/Array C and 492 kWh/Array B, due to a known diagram data outputs error swapping the data indicators of arrays B and C.

discrepancies is yet unknown. It is possible that denser interlayers of Array J featured strong light scattering losses at larger angles of sunlight incidence.

In order to more fully elucidate the interlayer composition-dependent energy-harvesting performance differences between different window design types, a “Test Window” was manufactured, which replicated the dimensions, PV circuitry, and internal glazing design structure of Murdoch greenhouse solar windows, except did not use any fluorescent materials added into its single PVB interlayer composition. Even though the interlayer composition and structure-related performance differences have been studied quite extensively using smaller lab-scale window samples, in a range of light incidence conditions, in both the natural sunlight and under solar simulator irradiation [24,25,35], it has been of interest to compare the daily energy outputs of greenhouse windows with an identical large-size reference solar window which did not employ any internal light redirection mechanisms in its design.

This Test Window was placed vertically in front of Room 2 between 19 December 2022 and early January 2023, to enable daily energy harvesting comparisons with 3 other window designs installed at north wall of greenhouse. Figure 12 shows the test window placement geometry

relatively to greenhouse wall; the nearby wall-based PV arrays design schematic is also shown.

The Test Window electric output at peak irradiation conditions (near midday on December 16, 2022), and at the optimum incidence angle was initially checked, with the expected parameters measured (V_{oc} near 58 V, max. I_{sc} of near 800 mA). After mounting the Test Window vertically onto testing frame in front of Room 2 windows, the output leads from this solar window were connected to the PV input of Victron SmartSolar MPPT charge controller. A semi-discharged 12 V, 10 Ah lead-acid battery was used as energy sink and to enable the energy flow measurements from the charger circuit (always kept in Bulk Charging mode), as well as to power the charge controller. The instantaneous PV power readings from Victron 75/10 were checked against the direct $I-V$ curve measurement data obtained from PROVA 200A Solar Module Analyzer, validating the power measurement data consistency. A Victron Cerbo-S GX data logger was configured to transmit the instantaneous PV input, MPPT charger circuit, battery state, and energy yield parameters online, to enable remote monitoring. Daily comparisons of the per-window harvested energy as well as the intra-day trends in power generation were made (for

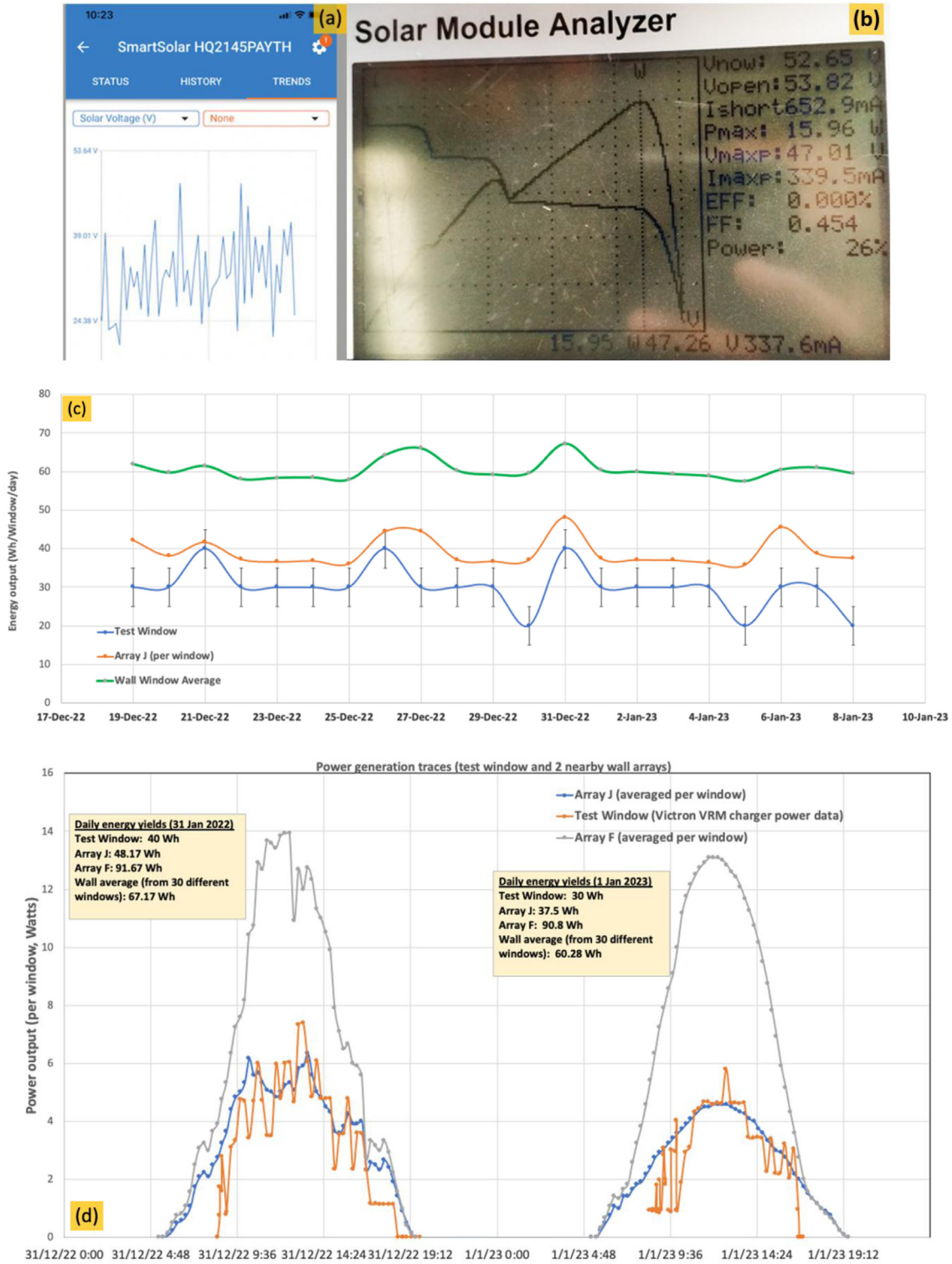


Fig. 13. Test Window electric output and daily energy monitoring results. (a) Instantaneous PV voltage variations (at MPPT, as monitored in real time by Victron 75/10 Charge Controller during morning hours); (b) an example I-V curve of a solar window with a low-quality interlayer measured with PROVA 200A PV Module Analyzer at close to optimum window orientation, featuring a distorted $I-V$ curve shape with side-peaks in the power-voltage curve; the output electric parameters also illustrate the significant reduction in the fill factor (FF) from its expected value of near 0.76; (c) daily energy output of Test Window measured by Victron 75/10, monitoring done for 21 days; data are plotted against the measured (per-window average) energy outputs of other solar windows installed in nearby wall arrays, and the wall average measured from 30 windows (arrays J, F, and C); (d) measured intra-day electric power output traces.

a 3-week period) with the windows from the nearby greenhouse wall arrays (Fig. 13).

A notable finding made using the real-time solar voltage output display of Victron charge controller was the identification of MPPT voltage jumps occurring on a fast time scale (each several seconds), between ~ 25 V and ~ 40 V, showing the instabilities in the maximum power point voltage of Test Window (Fig. 12a), resolved by the ultra-fast MPPT tracker circuit of Victron 75/10. PV Analyzer I - V curve measurements were slower (~ 5 s per scan), yet also showed the characteristic bending of the I - V curve shape, indicating unstable PV circuit operation typical of partially shaded electrically-mismatched complex-interconnected PV modules, and showing the presence of a side-peak in the power-voltage curve. Significant geometric shading was expected to affect a number of strip-shaped PV modules placed facing several different directions around the inner perimeter areas inside the Test Window, at least for a number of daylight hours, at light incidence angles well away from the normal incidence. This is because no internal light redistribution (or light diffusion) mechanisms were built-in, which could have otherwise made the light intensity distribution over the internal solar cell areas much more uniform, minimising the electric output mismatches between parts of the overall PV module circuit, and thus avoiding protective bypass diode circuitry activation, or the development of a lower-power peak voltage condition. The energy collection from any clear glass areas adjacent to solar cells has also been disabled in the Test Window design, which did not feature any light scattering or luminescence-assisted photon transport mechanisms, which are known to strongly improve the collection of obliquely-incident solar energy.

The Test Window has demonstrated a consistently much lower daily energy output, compared to the per-window energy yield data averaged between a total of 30 north wall windows (Fig 13c); it has also produced smaller daily energy yields than the nearby Array J windows, which were generating the smallest energy output among all wall window designs in summer. The midday peak power generation from the Test Window was very similar to windows of Array J, but much smaller than windows of Array F.

4 Conclusions

We have provided a review of the recent results in the field of high-transparency window-integrated PV and agrivoltaics, focussing on the datasets acquired during the performance monitoring of a solar window greenhouse constructed at Murdoch University. Solar glazing system development approaches and functional material systems used in window-based energy harvesting technologies have been described, with a brief review of their recent development history. An example agrivoltaic facility at Murdoch University Solar Greenhouse (Perth, Western Australia) and the observed trends in its energy generation and energy use performance have been described in detail.

The main findings related to the performance of Murdoch University Solar Greenhouse were as follows:

- accurate temperature control was demonstrated, maintaining microclimate at $\pm 2^\circ\text{C}$ from the required set-points, during both the daytime and night-time periods.
- the summer-season HVAC/greenhouse climate monitoring results have confirmed that the HVAC and IoT climate-control systems designed specifically for Murdoch Greenhouse by the Clearvue team were capable of providing the required fine climate control during the hot summer months in Perth. During the winter months, relatively small amounts of energy were used to provide the effective heating.
- electric energy production by multi-oriented window-integrated PV (WIPV) solar windows installation demonstrated to be in line with the expected performance;
- different window design types resulted in different energy harvesting performance characteristics (as was expected); the results of energy production monitoring will be utilised for further fine-tuning of the PVB interlayer recipes.
- high levels of energy self-sufficiency (averaging up to $\sim 40\%$, and up to $\sim 60\%$ demonstrated in window-integrated solar greenhouse on sunny autumn days in Perth), provided the most energy-efficient climate control algorithms were used.

The wide applications potential of this novel type of energy-generating transparent construction materials includes commercial buildings, public infrastructure, and agrivoltaics. We demonstrated that significant energy savings are possible in commercial greenhouses using high-transparency WIPV.

References

1. L. Capuano, International Energy Outlook 2018 (IEO2018), USS Energy Information Administration, Washington, DC, USA, 2018
2. E. Biyik, M. Araz, A. Hepbasli, M. Shahrestani, R. Yao, L. Shao, E. Essah, A.C. Oliveira, T. del Cano, E. Rico et al., A key review of building integrated photovoltaic (BIPV) systems, Eng. Sci. Technol. Int. J. **20**, 833–858 (2017)
3. M. Vasiliev, M., Nur-E-Alam, K. Alameh, Recent developments in solar energy-harvesting technologies for building integration and distributed energy generation, Energies **12**, 1080 (2019)
4. D. Moor, V. Rosenberg, M. Vasiliev, High transparency clear glass windows with large PV energy outputs, in: Proceedings of Challenging Glass Conference, Vol. **8**, 2022
5. T.E. Kuhn, C. Erban, M. Heinrich, J. Eisenlohr, F. Ennslen, D.H. Neuhaus, Review of technological design options for building integrated photovoltaics (BIPV), Energy Build. **231**, 110381 (2021)
6. N. Martín-Chivelet, K., Kapsis, H.R. Wilson, V. Delisle, R. Yang, L. Olivieri et al., Building-integrated photovoltaic (BIPV) products and systems: a review of energy-related behavior, Energy Build. **262**, 111998 (2022)
7. A. Taser, B.K. Koyunbaba, T. Kazanasmaz, Thermal, daylight, and energy potential of building-integrated photovoltaic (BIPV) systems: a comprehensive review of effects and developments, Solar Energy **251**, 171–196 (2023)

8. Z.R.K. Abojela, M.K. MatDesa, A.H. Sabry, Current prospects of building-integrated solar PV systems and the application of bifacial PVs, *Front. Energy Res.* **11**, 1164494 (2023)
9. Y. Li, L. Li, W. Deng, D. Zhu, L. Hong, Building integrated photovoltaic (BIPV) development knowledge map: a review of visual analysis using CiteSpace, *Buildings* **13**, 389 (2023)
10. C. Toledo, A. Scognamiglio, Agrivoltaic systems design and assessment: a critical review, and a descriptive model towards a sustainable landscape vision (three-dimensional agrivoltaic patterns), *Sustainability* **13**, 6871 (2021)
11. M.A. AlMamun, P. Dargusch, D. Wadley, N.A. Zulkarnain, A.A. Aziz, A review of research on agrivoltaic systems, *Renew. Sustain. Energy Rev.* **161**, 112351 (2022)
12. A.V. Klokov, E.Y. Loktionov, Y.V. Loktionov, V.A. Panchenko, E.S. Sharaborova, A mini-review of current activities and future trends in agrivoltaics, *Energies* **16**, 3009 (2023)
13. Clearvue Technologies website <https://www.clearvuepv.com/frequently-asked-questions/> (accessed on 12 October 2022)
14. M.G. Debije, P.P.C. Verbunt, Thirty years of luminescent solar concentrator research: solar energy for the built environment, *Adv. Energy Mater.* **2**, 12–35 (2012)
15. M.G. Debije, V.A. Rajkumar, Direct versus indirect illumination of a prototype luminescent solar concentrator, *Solar Energy* **122**, 334–340 (2015)
16. L. Desmet, A.J.M. Ras, D.K.G. de Boer, M.G. Debije, Monocrystalline silicon photovoltaic luminescent solar concentrator with 4.2% power conversion efficiency, *Opt. Lett.* **37**, 3087–3089 (2012)
17. A. Reinders, R. Kishore, L. Slooff, W. Eggink, Luminescent solar concentrator photovoltaic designs, *Jpn. J. Appl. Phys.* **57**, 08RD10 (2018)
18. B. Zhang, G. Lyu, E.A. Kelly, R.C. Evans, Förster resonance energy transfer in luminescent solar concentrators, *Adv. Sci.* **9**, 2201160 (2022)
19. T. Warner, K.P. Ghiggino, G. Rosengarten, A critical analysis of luminescent solar concentrator terminology and efficiency results, *Solar Energy* **246**, 119–140 (2022)
20. Device for generating electric energy, US Patent US 1116 2302B2, <https://patents.google.com/patent/US11162302B2/en>
21. M. Vasiliev, K. Alameh, M. Nur-E-Alam, Spectrally-selective energy-harvesting solar windows for public infrastructure applications, *Appl. Sci.* **8**, 849 (2018)
22. M. Vasiliev, M. Nur-E-Alam, K. Alameh, Initial field testing results from building-integrated solar energy harvesting windows installation in Perth, Australia, *Appl. Sci.* **9**, 4002 (2019)
23. H. Li, K. Wu, J. Lim, H.-J. Song, V.I. Klimov, Doctor-blade deposition of quantum dots onto standard window glass for low-loss large-area luminescent solar concentrators. *Nat. Energy* **16157** (2016).
24. M. Vasiliev, R. Alghamedi, M. Nur-E-Alam, K. Alameh, Photonic microstructures for energy-generating clear glass and net-zero energy buildings, *Sci. Rep.* **6**, 31831 (2016)
25. R. Alghamedi, M. Vasiliev, M. Nur-E-Alam, K. Alameh, Spectrally-selective all-inorganic scattering luminophores for solar energy-harvesting clear glass windows, *Sci. Rep.* **4**, 6632 (2014)
26. A.M. Ramachandran, M.S. Sangeetha, A.S. Thampi, M. Singh, A. Asok, A comprehensive review on optics and optical materials for planar waveguide-based compact concentrated solar photovoltaics, *Results Eng.* **16**, 100665 (2022)
27. Y. You, X. Tong, A.I. Channa, H. Zhi, M. Cai, H. Zhao, L. Xia, G. Liu, H. Zhao, Z. Wang, High-efficiency luminescent solar concentrators based on Composition-tunable Eco-friendly Core/shell quantum dots, *Chem. Eng. J.* **452**, 139490 (2023)
28. C. Yang, R.R. Lunt, Limits of visibly transparent luminescent solar concentrators, *Adv. Opt. Mater.* **5**, 1600851 (2017)
29. S. Ren, C. Shou, S. Jin, G. Chen, S. Han, Z. Chen, X. Chen, S. Yang, Y. Guo, C.-C. Tu, Silicon quantum dot luminescent solar concentrators and downshifters with antireflection coatings for enhancing perovskite solar cell performance, *ACS Photonics* **8**, 2392–2399 (2021)
30. M. Aghaei, R. Pelosi, W.W.H. Wong, T. Schmidt, M.G. Debije, A.H.M.E. Reinders, Measured power conversion efficiencies of bifacial luminescent solar concentrator photovoltaic devices of the mosaic series, *Progr. Photovoltaics Res. Appl.* **30**, 726–739 (2022)
31. R.A.S. Ferreira, S.F.H. Correia, A. Monguzzi, X. Liu, F. Meinardi, Spectral converters for photovoltaics—what’s ahead, *Mater. Today* **33**, 105–121 (2020)
32. F. Zhang, J. Bao, C. Gao, Design and optimization of transparent scattering solar concentrator based on SiO₂ aerogel, *JUSTC* **52**, 2 (2022)
33. E. Ela, V. Diakov, E. Ibanez, M. Heaney, Impacts of variability and uncertainty in solar photovoltaic generation at multiple timescales, Technical Report NREL/TP- 5500 -58274, NREL, Golden, Colorado, USA, 2013
34. M.A. Imteaz, A. Ahsan, Solar panels: real efficiencies, potential productions and payback periods for major Australian cities, *Sust. Energy Technol. Assessm.* **25**, 119–125 (2018)
35. M. Vasiliev, K. Alameh, M.A. Badshah, S.-M. Kim, M. Nur-E-Alam, Semi-transparent energy-harvesting solar concentrator windows employing infrared transmission-enhanced glass and large-area microstructured diffractive elements, *Photonics* **5**, 25 (2018)

Citation de l’article: Mikhail Vasiliev, Victor Rosenberg, David Goodfield, Jamie Lyford, Chengdao Li, High-transparency clear window-based agrivoltaics, *Sust. Build.* **6**, 5 (2023)